arXiv:1511.02762v1 [physics.gen-ph] 27 Oct 2015

Dynamics of Scalar Thin-Shell for a Class of Regular Black Holes

M. Sharif[1] *and Sehrish Iftikhar [1,2] †
[1] Department of Mathematics, University of the Punjab,
Quaid-e-Azam Campus, Lahore-54590, Pakistan.
[2]Department of Mathematics, Lahore College
for Women University, Lahore-54000, Pakistan.

Abstract

This paper is devoted to study the dynamical behavior of thin-shell composed of perfect fluid by considering matter field as a scalar field. We formulate equation of motion of the shell by using Israel thin-shell formalism for a class of regular black holes as interior and exterior regions. The corresponding scalar fields and effective potentials are investigated numerically for both massless and massive scalar fields. We conclude that massless scalar shell leads to collapse, expansion and equilibrium while the massive case leads to collapse only.

Keywords: Gravitational collapse; Scalar field; Israel thin-shell formalism.
PACS: 04.20.-q; 04.40.Dg; 04.70.Bw; 75.78.-n

1 Introduction

Scalar fields play a key role in several astrophysical phenomena and have many applications in theoretical physics, cluster dynamics and cosmology. Wheeler (1955) found particle like solutions (geons) from classical electromagnetic field coupled to general relativity (GR) which were extended by

*msharif.math@pu.edu.pk
†sehrish3iftikhar@gmail.com

Brill and Wheeler (1957) as well as by Frederick (1957). Bergmann and Leipnik (1957) investigated solution of the Einstein field equations in the presence of scalar field for Schwarzschild geometry. Christodoulou (1991) examined spherically symmetric scalar collapse and formation of singularities. Choptuik (1993) studied spherically symmetric collapse of a massless scalar field minimally coupled with gravity and discussed its solutions numerically. Harada et al. (1997) investigated collapsing compact object in scalar-tensor theory which predicts the existence of scalar gravitational waves.

The study of dynamics of an astrophysical object with scalar field has been the subject of keen interest for many people. Kaup (1968) as well as Ruffini and Bonazzola (1969) were the pioneers to study boson stars (composed of self-gravitating complex scalar field). Gleiser (1988) investigated the dynamical instability of boson stars and concluded that instabilities do not occur for the critical centra1 density but for centra1 densities considerably higher. Seidel and Suen (1990) examined dynamical evolution of boson stars using perturbation and discussed the existence as well as formation of boson stars. Siebel et al. (2001) studied dynamics of massless scalar field interacting with a self-gravitating neutron star and found that the scalar wave forces the neutron star either to oscillate or to undergo gravitational collapse to form a black hole (BH) on a dynamical timescale. Bhattacharya et al. (2009) explored spherically symmetric collapse of a massless scalar field and discussed possibility for the existence of a class of nonsingular models.

Chase (1970) examined instability of spherically symmetric charged fluid shell by using equation of state. Boulware (1973) investigated time evolution of the charged thin-shell and found that end state of collapse could be a naked singularity if and only if density is negative. Barrabès and Israel (1991) studied dynamics of thin-shells traveling at the speed of light. *Núñez* et al. (1997) investigated stability and dynamical behavior of a real scalar field for the Schwarzschild BH. Goncalves (2002) examined dynamical properties of timelike thin-shell by using Israel formalism and formulated necessary and sufficient condition for the shell crossing. Oren and Piran (2003) explored evolution of a charged spherical shell of massless scalar fields numerically. Crisostomo and Olea (2004) used Hamiltonian treatment to study gravitational collapse of thin shells. Recently, Sharif and Abbas (2012) explored the dynamics of scalar field charged thin-shell and concluded that for both (massless and massive scalar fields) shell can expand to infinity or collapse to zero size forming a curvature singularity or bounce under suitable conditions. Many interesting results regarding thin-shell formalism can be found in lit-

erature (Sharif and Ahmad 2008; Sharif and Iqbal 2009; Sharif and Abbas 2011).

It is well-known that BH solutions (Schwarzschild, Reissner-Nordström (RN), Kerr and Kerr-Newman) contain curvature singularity beyond their event horizons. A comprehensive understanding of BH requires singularity-free solutions. Black holes having regular centers are called regular or non-singular BHs. Regular BHs are static and asymptotically flat, satisfying the weak energy condition. These are exact solutions of the Einstein field equations for which singularity is avoided in the presence of horizons (the exterior Schwarzschild-like horizon and an interior de-Sitter-like horizon). The first regular BH was introduced by Bardeen (1968) which has both event (exterior) and Cauchy (interior) horizons, but with a regular center. Bardeen BH can be interpreted as a magnetic solution of the Einstein equations coupled to nonlinear electrodynamics where singularity is replaced by a de Sitter core. Later, many spherically symmetric regular BH solutions were found based on Bardeen's proposal (Borde 1997; Ayon-Beato and Garcia 1998; Bronnikov 2000, 2001). Further analysis of singularity avoidance has been proposed by Hayward (2006). This BH consists of a compact spacetime region of trapped surfaces, with inner and outer boundaries which join circularly as a single smooth trapping horizon

The purpose of this paper is to study the dynamical effects of scalar field on magnetically charged thin-shell using Israel thin-shell formalism for a class of regular BHs. The format of the paper is as follows. In the next section, we derive equation of motion for the thin-shell using Israel formalism. Section **3** investigates the equation of motion for a class of regular BHs for both massless and massive scalar fields. Final remarks are given in the last section.

2 Thin-Shell Formalism and Equation of Motion

Thin-shell formalism (Israel 1966, 1967) has extensively been used to study the dynamics of matter fields, wormholes, collision of shells, interior structure of BHs, bubble dynamics and inflationary scenarios. In this method, surface properties are described in terms of jump of the extrinsic curvature (functions of intrinsic coordinates of the layer) across the boundary layer.

This formalism allows to choose four-dimensional coordinates independently on both sides of the boundary layer. The governing equations resulting from this formalism correspond to the equation of motion whose solution can completely describe the dynamics of the shell.

We assume three-dimensional timelike boundary surface Σ, which splits spherically symmetric spacetime into two four-dimensional manifolds N^+ and N^-. The interior and exterior regions are described by a metric of the form

$$ds^2 = F_{\pm}(R)dT^2 - F_{\pm}^{-1}(R)dR^2 - R^2(d\theta^2 + \sin^2\theta d\varphi^2), \tag{1}$$

where explicit forms of $F(R)$ distinguish between different spacetime geometries. In this paper, we shall use the following choices of this function.

Table 1: Regular BHs.

Name of Regular BH	$F(R)$
Bardeen	$F_{\pm1}(R) = 1 - \frac{2M_{\pm}R^2}{(R^2+e_{\pm}^2)^{\frac{3}{2}}}$
Hayward	$F_{\pm2}(R) = 1 - \frac{2M_{\pm}R^2}{R^3+2e_{\pm}^2}$
ABGB	$F_{\pm3}(R) = 1 - \frac{2M_{\pm}R^2}{(R^2+e_{\pm}^2)^{\frac{3}{2}}} + \frac{e_{\pm}^2R^2}{(R^2+e_{\pm}^2)^2}$

where $M_{\pm}$ and $e_{\pm}$ are the mass and monopole charge of a self-gravitating magnetic field of a non-linear electrodynamics source, respectively. All the above BH solutions correspond to the Schwarzschild BH for $e = 0$. Moreover, it is assumed that the interior region contains more mass than the exterior region, i.e., gravitational masses are unequal $M_- \neq M_+$ while charge is uniformly distributed in both regions, i.e., $e = e_- = e_+$. By applying the intrinsic coordinates $(\tau,\ \theta,\ \varphi)$ on the hypersurface (Σ) at $R = R(\tau)$, Eq.(1) becomes

$$(ds)^2_{\pm\Sigma} = \left[F_{\pm}(R) - F_{\pm}^{-1}(R)(\frac{dR}{d\tau})^2(\frac{d\tau}{dT})^2\right]dT^2 - R^2(\tau)(d\theta^2 + \sin^2\theta d\varphi^2). \tag{2}$$

Here, it is assumed that $T(\tau)$ is a timelike coordinate, i.e., $g_{00} > 0$. Also, the induced metric on the boundary surface is given as

$$(ds)^2 = d\tau^2 - \alpha^2(\tau)(d\theta^2 + \sin^2\theta d\varphi^2). \tag{3}$$

The continuity of first fundamental forms give

$$\left[F_{\pm}(R) - F_{\pm}^{-1}(R)(\frac{dR}{d\tau})^2(\frac{d\tau}{dT})^2\right]^{\frac{1}{2}}dT = (d\tau)_{\Sigma}, \quad R(\tau) = \alpha(\tau)_{\Sigma}. \tag{4}$$

The outward unit normals $\eta_\mu^\pm$ in $N^\pm$ coordinates are calculated as

$$\eta_\mu^\pm = (-\dot{R}, \dot{T}, 0, 0),$$

where dot represents differentiation with respect to τ. The surface stress energy-momentum tensor is defined as

$$S_{\mu\nu} = \frac{1}{\kappa}([K_{\mu\nu}] - \gamma_{\mu\nu}[K]), \tag{5}$$

where $\gamma_{\mu\nu}$ denotes the induced metric, κ is the coupling constant and

$$[K_{\mu\nu}] = K^+_{\mu\nu} - K^-_{\mu\nu}, \quad [K] = \gamma^{\mu\nu}[K_{\mu\nu}]. \tag{6}$$

The non-vanishing components of extrinsic curvature are

$$K^\pm_{\tau\tau} = \frac{d}{dR}\sqrt{\dot{R}^2 + F_\pm}, \quad K^\pm_{\theta\theta} = -R\sqrt{\dot{R}^2 + F_\pm}, \quad K^\pm_{\varphi\varphi} = \sin^2\theta K^\pm_{\theta\theta}. \tag{7}$$

The surface stress energy-momentum tensor for a perfect fluid is

$$S_{\mu\nu} = (\rho + p)u_\mu u_\nu - p\gamma_{\mu\nu}, \tag{8}$$

where ρ is the energy density, p is the isotropic pressure and $u_\mu = \delta^0_\mu$ is the velocity of the shell. Using Eqs.(4), (5) and (8), we find

$$\rho = \frac{2}{\kappa R^2}[K_{\theta\theta}], \quad p = \frac{1}{\kappa}([K_{\tau\tau}] - \frac{[K_{\theta\theta}]}{R^2}). \tag{9}$$

Using Eq.(7) in (9), we can obtain the following relations

$$(\omega_+ - \omega_-) + \frac{\kappa}{2}\rho R = 0, \tag{10}$$

$$\frac{d}{dR}(\omega_+ - \omega_-) + \frac{1}{R}(\omega_+ - \omega_-) - \kappa p = 0, \tag{11}$$

where $\omega_\pm = \sqrt{\dot{R}^2 + F_\pm}$.

The above equations lead to the following differential equation

$$\frac{d\rho}{dR} + \frac{2}{R}(\rho + p) = 0, \tag{12}$$

which is equivalent to the energy conservation of the thin-shell

$$\dot{m} + p\dot{A} = 0, \tag{13}$$

where $m=\rho A$ and $A=4\pi R^2(\tau)$ represent mass and area of the shell, respectively. It is mentioned here that Eq.(12) can be solved using the equation of state $p=\check{k}\rho$ whose solution is

$$\rho=\rho_0\left(\frac{R_0}{R}\right)^{2(\check{k}+1)}, \tag{14}$$

where R_0 represents initial position of the shell at time $\tau=\tau_0$ and ρ_0 denotes matter density of the shell at R_0. Using the above equation, the mass of the shell takes the form

$$m=4\pi\rho_0\frac{R_0^{2(\check{k}+1)}}{R^{2\check{k}}}. \tag{15}$$

Equation (10) leads to the equation of motion of the shell

$$\dot{R}^2+V_{eff}=0, \tag{16}$$

where

$$V_{eff}(R)=\frac{1}{2}(F_++F_-)-\frac{(F_++F_-)^2}{(\kappa\rho R)^2}-\frac{1}{16}(\kappa\rho R)^2, \tag{17}$$

is the effective potential which describes shell's motion.

3 Analysis of Equation of Motion

Here we study the dynamical behavior of the scalar shell for a family of regular BHs. For this purpose, we first calculate the effective potential and the corresponding velocity of the shell with respect to the stationary observer. We investigate the effect of charge parameter on the dynamics of the shell.

3.1 Bardeen Regular BH

Bardeen (1968) found a solution of the field equations having an event horizon but excluding a singularity at the origin. This solution is parameterized by mass M and monopole charge e of a self-gravitating magnetic field described by nonlinear electrodynamics which is well-defined for $R\geq 0$, behaves like de Sitter black hole for $R\to 0$ and asymptotically as the RN solution. The corresponding effective potential is

$$V_{eff_{(1)}}(R)=1-\left(\frac{2R^3}{(R^2+e^2)^{\frac{3}{2}}}\right)^2\left(\frac{M_+-M_-}{m}\right)^2-\frac{(M_++M_-)R^2}{(R^2+e^2)^{\frac{3}{2}}}-\left(\frac{m}{2R}\right)^2. \tag{18}$$

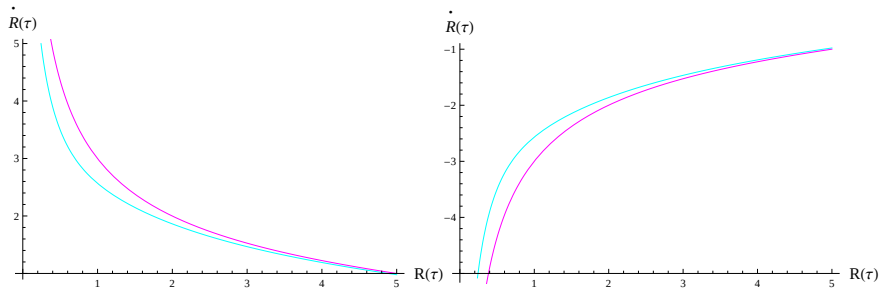

Figure 1: Plots of $\dot{R}(\tau)$ versus R for Bardeen BH when $M_- = 0$, $M_+ = 1$, $R_0 = \rho_0 = \check{k} = 1$ and $e = 1$. Here $M_+ = 1$ corresponds to mass of the exterior BH while $M_- = 0$ denotes the interior flat geometry. Left and right graphs describe the case of expansion and collapse while blue and purple curves correspond to charge and uncharged shell.

To examine the effect of charge on the shell's dynamics, Eq.(16) can be written as

$$\dot{R} = \pm \left[\left(\frac{2R^3}{(R^2+e^2)^{\frac{3}{2}}} \right)^2 \frac{(M_+ - M_-)^2}{m^2} + \frac{(M_+ + M_-)R^2}{(R^2+e^2)^{\frac{3}{2}}} + \left(\frac{m}{2R} \right)^2 - 1 \right]^{\frac{1}{2}}. \tag{19}$$

Here $-(+)$ correspond to collapse (expansion) of the shell. In Figure **1**, the left graph represents $\dot{R} > 0$ while the right graph shows the behavior of shell's velocity as $\dot{R} < 0$. In the first case, the velocity of the shell decreases positively while in the second case, it increases negatively. We also see that velocity of the charged (regular) shell is less than the uncharged (singular) in both cases and also both curves match for the large radius.

3.2 Hayward BH

Hayward (2006) found a simple regular BH solution in which e is related to the cosmological constant Λ as $e^2 = \frac{3M}{\Lambda}$ and for the well-defined asymptotic limits, this corresponds to the Schwarzschild BH as $R \to \infty$ while it becomes de Sitter spacetime at the center ($R \to 0$). The corresponding effective

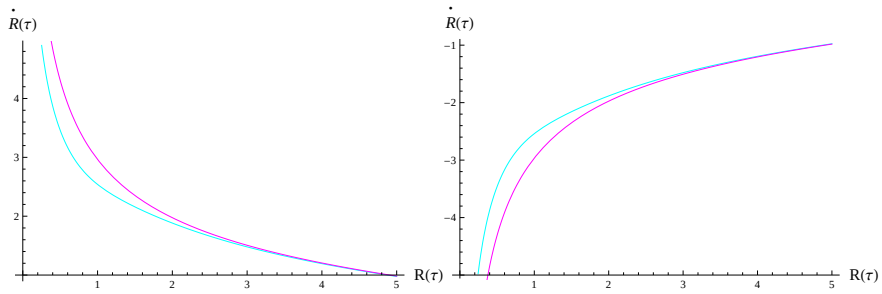

Figure 2: Plots of $\dot{R}(\tau)$ versus R for Hayward BH.

potential is

$$V_{eff_{(2)}}(R) = 1 - \left(\frac{2R^3}{R^3+2e^2}\right)^2 \left(\frac{M_+ - M_-}{m}\right)^2 - \frac{(M_+ + M_-)R^2}{(R^3+2e^2)} - \left(\frac{m}{2R}\right)^2. \tag{20}$$

Equation (16) and (20) yield

$$\dot{R} = \pm \left[\left(\frac{2R^3}{R^3+2e^2}\right)^2 \left(\frac{M_+ - M_-}{m}\right)^2 + \frac{(M_+ + M_-)R^2}{R^3+2e^2} + \left(\frac{m}{2R}\right)^2 - 1\right]^{\frac{1}{2}}. \tag{21}$$

Figure **2** shows the same behavior of velocity as for Bardeen regular BH.

3.3 Ayon-Beato and Garcia and Bronnikov BH

Another interesting model of non-linear electrodynamics coupled with GR was proposed by Ayon-Beato and Garcia (1998) and Bronnikov (2000, 2001) (ABGB). This is singularity free BH for a nonlinear magnetic monopole which behaves asymptotically as RN solution. The corresponding effective potential is

$$\begin{aligned} V_{eff_{(3)}}(R) &= 1 - \left(\frac{2R^3}{(R^2+e^2)^{\frac{3}{2}}}\right)^2 \left(\frac{M_+ - M_-}{m}\right)^2 - \frac{(M_+ + M_-)R^2}{(R^2+e^2)^{\frac{3}{2}}} \\ &+ \frac{e^2R^2}{(R^2+e^2)^2} - \left(\frac{m}{2R}\right)^2. \end{aligned} \tag{22}$$

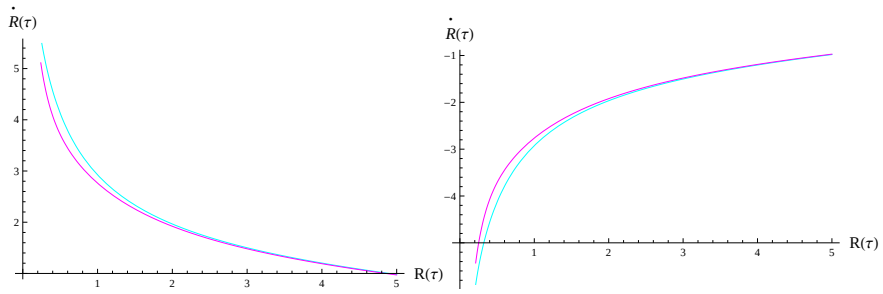

Figure 3: Plots of $\dot{R}(\tau)$ versus R for ABGB BH.

Solving Eqs.(16) and (22), we obtain

$$\dot{R} = \pm\left[\left(\frac{2R^3}{(R^2+e^2)^{\frac{3}{2}}}\right)^2\frac{(M_+-M_-)^2}{m^2}+\frac{(M_++M_-)R^2}{(R^2+e^2)^{\frac{3}{2}}}\right.$$
$$\left. - \frac{e^2R^2}{(R^2+e^2)^2}+\left(\frac{m}{2R}\right)^2-1\right]^{\frac{1}{2}}. \tag{23}$$

This also shows the same behavior as for Bardeen regular BH (Figure: **1**).

3.4 Dynamics of Scalar Shell

In this section, we study the dynamics of thin-shell with the scalar field. For this purpose, we obtain the energy-momentum tensor for the scalar field by applying a transformation on Eq.(8) given as (Núñez 1998)

$$u_\mu = \frac{\varphi_{,\mu}}{\sqrt{\varphi_{,\nu}\varphi^{,\nu}}}, \quad \rho = \frac{1}{2}[\varphi_{,\nu}\varphi^{,\nu}+2V(\varphi)], \quad p = \frac{1}{2}[\varphi_{,\nu}\varphi^{,\nu}-2V(\varphi)], \tag{24}$$

where $V(\varphi)=m^2\varphi^2$ is the potential term representing a massive scalar field. In the absence of this term, the scalar field will become massless. From Eqs.(8) and (24), the energy-momentum tensor for the scalar field can be written as

$$S_{\mu\nu} = \nabla_\mu\varphi\nabla_\nu\varphi - \gamma_{\mu\nu}[\frac{1}{2}(\nabla\varphi)^2 - V(\varphi)].$$

Since the induced metric is a function of τ only, so φ also depends on τ. Thus Eq.(24) takes the form

$$\rho = \frac{1}{2}[\dot{\varphi}^2+2V(\varphi)], \quad p = \frac{1}{2}[\dot{\varphi}^2-2V(\varphi)]. \tag{25}$$

The total mass of the scalar shell can be written as

$$m = 2\pi R^2[\dot{\varphi} + 2V(\varphi)]. \tag{26}$$

Inserting Eqs.(25) and (26) in (13), we obtain

$$\ddot{\varphi} + \frac{2\dot{R}}{R}\dot{\varphi} + \frac{\partial V}{\partial \varphi} = 0, \tag{27}$$

which is the Klien-Gordon (KG) equation, $\Box\varphi + \frac{\partial V}{\partial \varphi} = 0$, written in shell's coordinate system.

The effective potentials for the Bardeen, Hayward and ABGB BHs in terms of scalar field are obtained as

$$\begin{aligned} V_{eff_{(1)}}(R) &= 1 - \left(\frac{2R^3}{(R^2+e^2)^{\frac{3}{2}}}\right)^2 \left(\frac{M_+ - M_-}{2\pi R^2(\dot{\varphi} + 2V(\varphi))}\right)^2 \\ &- \frac{(M_+ + M_-)R^2}{(R^2+e^2)^{\frac{3}{2}}} - [\pi R(\dot{\varphi} + 2V(\varphi))]^2, \end{aligned} \tag{28}$$

$$\begin{aligned} V_{eff_{(2)}}(R) &= 1 - \left(\frac{2R^3}{R^3+2e^2}\right)^2 \left(\frac{M_+ - M_-}{2\pi R^2(\dot{\varphi} + 2V(\varphi))}\right)^2 \\ &- \frac{(M_+ + M_-)R^2}{(R^3+2e^2)} - [\pi R(\dot{\varphi} + 2V(\varphi))]^2, \end{aligned} \tag{29}$$

$$\begin{aligned} V_{eff_{(3)}}(R) &= 1 - \left(\frac{2R^3}{(R^2+e^2)^{\frac{3}{2}}}\right)^2 \left(\frac{M_+ - M_-}{2\pi R^2(\dot{\varphi} + 2V(\varphi))}\right)^2 \\ &- \frac{(M_+ + M_-)R^2}{(R^2+e^2)^{\frac{3}{2}}} + \frac{e^2R^2}{(R^2+e^2)^2} - [\pi R(\dot{\varphi} + 2V(\varphi))]^2. \end{aligned} \tag{30}$$

Now we solve Eqs.(16) and (27) with the help of Eqs.(28)-(30). These equations cannot be solved analytically, so we solve them numerically, assuming $M_- = 0,\ M_+ = 1,\ R_0 = \rho_0 = \check{k} = 1,\ e = 1$ and $m = 1$ which are shown in Figures **4** and **5**. The behavior of shell's radius is represented in Figure **4** for Bardeen, Hayward and ABGB BHs. The upper and lower curves represent expanding and collapsing shell which describe the motion of the shell. For Bardeen BH, the upper curve starts with a static configuration then expands forever, while the lower curve represents that the shell radius starts with a uniform motion then decreases infinitely on the negative axis. In the plots of

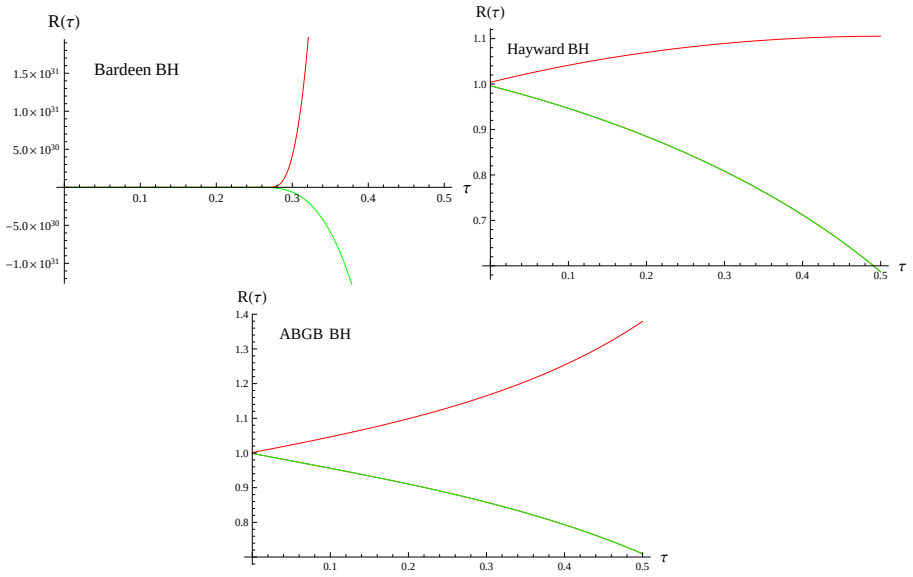

Figure 4: Plots of shell's radius with scalar field.

radii for Hayward and ABGB BHs, the upper curves indicate that the shell expands endlessly and the lower curve shows that the radius is decreasing continuously. Figure **5** describes solutions of the KG equation (27) for the same BHs. The upper curves represent collapsing while the lower curves show the expanding scalar shell. The scalar field density is increasing in the first case (collapse) while it decays to zero as time increases in the second case (expansion).

3.4.1 Massless Scalar Shell

Here we investigate dynamics of the shell in the absence of $V(\varphi)$, i.e., the massless scalar field. In this case, KG equation becomes $\ddot{\varphi} + \frac{2\dot{R}}{R}\dot{\varphi} = 0$, and its integration leads to $\dot{\varphi} = \frac{\lambda}{R^2}$, where λ is an integration constant. The corresponding equations of motion for the Bardeen, Hayward and ABGB

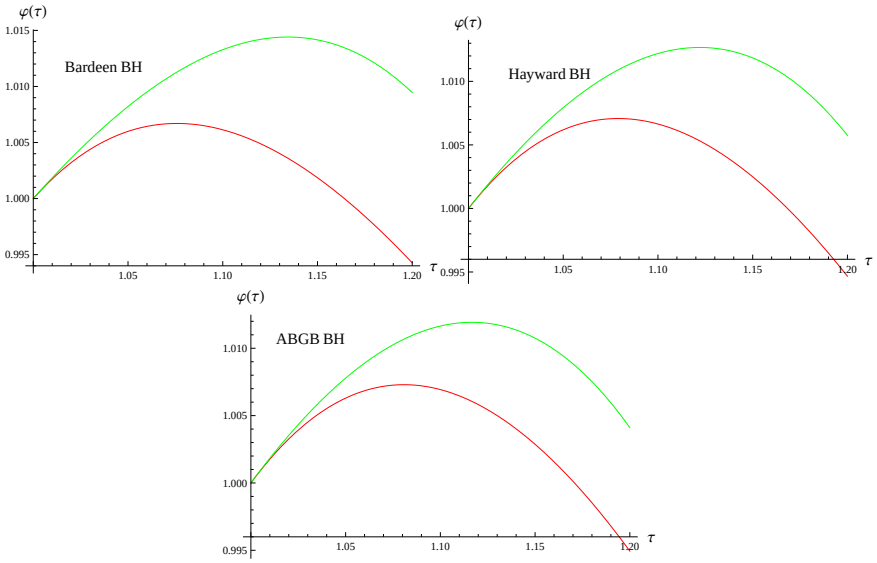

Figure 5: Plots of the scalar field. Green and red curves correspond to collapse and expansion.

BHs with Eq.(28)-(30) become

$$\dot{R}^2 + 1 - \left(\frac{2R^5}{(R^2+e^2)^{\frac{3}{2}}}\right)^2 \left(\frac{M_+ - M_-}{2\pi\lambda^2}\right)^2 - \frac{(M_+ + M_-)R^2}{(R^2+e^2)^{\frac{3}{2}}} - \left(\frac{\pi\lambda^2}{R^3}\right)^2 = 0, \tag{31}$$

$$\dot{R}^2 + 1 - \left(\frac{2R^5}{R^3+2e^2}\right)^2 \left(\frac{M_+ - M_-}{2\pi\lambda^2}\right)^2 - \frac{(M_+ + M_-)R^2}{R^3+2e^2} - \left(\frac{\pi\lambda^2}{R^3}\right)^2 = 0, \tag{32}$$

$$\dot{R}^2 + 1 - \left(\frac{2R^5}{(R^2+e^2)^{\frac{3}{2}}}\right)^2 \left(\frac{M_+ - M_-}{2\pi\lambda^2}\right)^2 - \frac{(M_+ + M_-)R^2}{(R^2+e^2)^{\frac{3}{2}}} + \frac{e^2R^2}{(R^2+e^2)^2} - \left(\frac{\pi\lambda^2}{R^3}\right)^2 = 0. \tag{33}$$

These can be simplified by using the parameters

$$[M] = M_+ - M_-, \quad \bar{M} = \frac{M_+ + M_-}{2}. \tag{34}$$

Inserting these parameters in Eqs.(31)-(33), we have

$$\dot{R}^2 + V_{eff} = 0, \tag{35}$$

where

$$V_{eff_{(1)}}(R) = 1 - \left(\frac{2R^5}{(R^2+e^2)^{\frac{3}{2}}}\right)^2 \left(\frac{[M]}{2\pi\lambda^2}\right)^2 - \frac{(2\bar{M})R^2}{(R^2+e^2)^{\frac{3}{2}}} - \left(\frac{\pi\lambda^2}{R^3}\right)^2, \tag{36}$$

$$V_{eff_{(2)}}(R) = 1 - \left(\frac{2R^5}{R^3+2e^2}\right)^2 \left(\frac{[M]}{2\pi\lambda^2}\right)^2 - \frac{(2\bar{M})R^2}{R^3+2e^2} - \left(\frac{\pi\lambda^2}{R^3}\right)^2, \tag{37}$$

$$V_{eff_{(3)}}(R) = 1 - \left(\frac{2R^5}{(R^2+e^2)^{\frac{3}{2}}}\right)^2 \left(\frac{[M]}{2\pi\lambda^2}\right)^2 - \frac{(2\bar{M})R^2}{(R^2+e^2)^{\frac{3}{2}}} + \frac{e^2R^2}{(R^2+e^2)^2} - \left(\frac{\pi\lambda^2}{R^3}\right)^2. \tag{38}$$

In Figures **6-11**, we examine numerical results for the massless scalar field using $M_- = 0$, $M_+ = 1$, R_0, $e = 1$ and $\lambda = 1$. Figure **6** shows that increasing and decreasing shell radius lead to expansion and collapse, respectively. The behavior of the effective potential is presented in Figure **7** which is divided into two regions. The upper region has a positive potential that leads to expansion. There is a turning (saddle) point where $V_{eff} = 0$, the shell stops for a while and then changes its behavior at $R = 3.5$ for Bardeen and Hayward BHs while at $R \approx 4$ for ABGB BH. The effective potential decreases infinitely after these points and becomes negative. This suggests that for large values of R the shell begins to contract continuously. Figures **8** and **9** describe behavior of the effective potential by varying M_+ and M_-. The saddle point ($V_{eff} = 0$) separates shell's motion into two regions: the upper (positive) and lower (negative) regions describe expansion and contraction of the shell, respectively. Figures **10** and **11** represent the behavior of effective potential by varying charge and λ. Again, the shell depicts three types of motion, expands in the upper region ($V_{eff} > 0$), in equilibrium position ($V_{eff} = 0$) and in the lower region the effective potential diverges negatively which leads the shell to collapse.

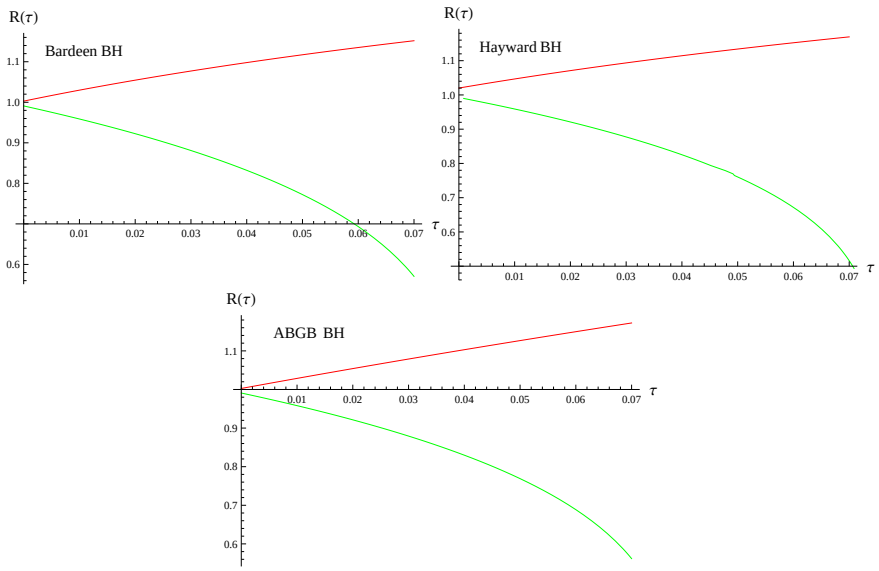

Figure 6: Behavior of radius of the massless scalar shell.

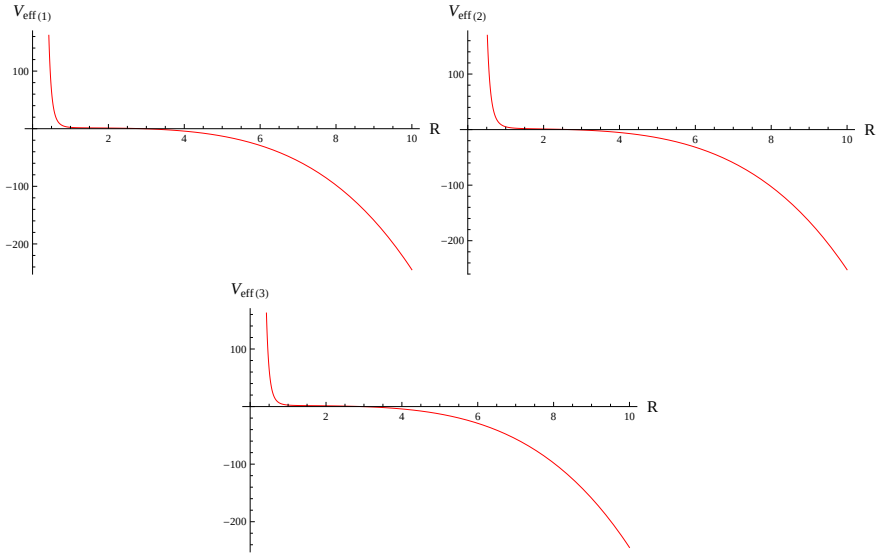

Figure 7: Plots of V_{eff} versus R for the massless case. In the upper panel, the left and right graphs show the plots for Bardeen and Hayward BHs while the lower panel represents ABGB BH for fixed M_- and M_+.

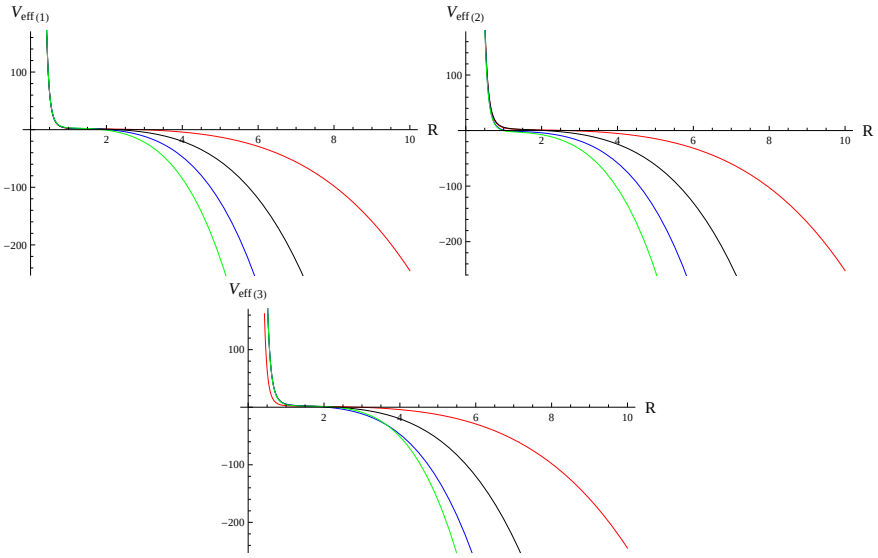

Figure 8: Behavior of V_{eff} of the massless shell by varying M_+.

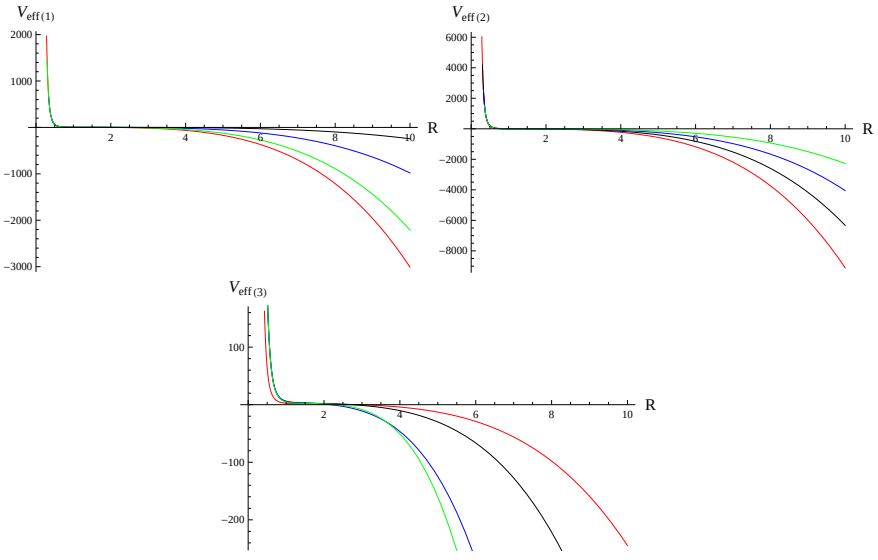

Figure 9: Behavior of V_{eff} of the massless shell by varying M_-.

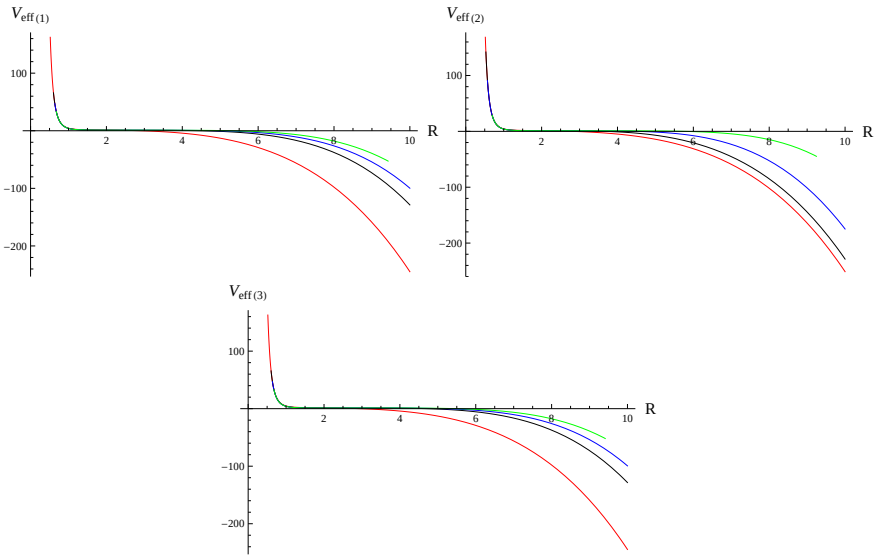

Figure 10: Behavior of V_{eff} of the massless shell by varying e.

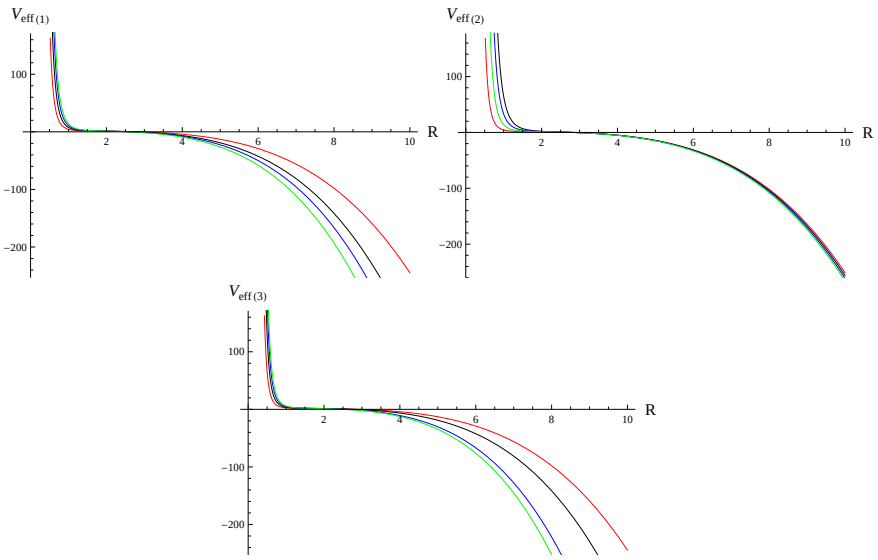

Figure 11: Behavior of V_{eff} of the massless shell by varying λ.

3.4.2 Massive Scalar Shell

Here we discuss the case when the thin-shell is composed of a massive scalar field with scalar potential. From Eq.(25), we obtain

$$\dot{\varphi}^2=\rho+p,\quad V(\varphi)=\frac{1}{2}(p-\rho). \tag{39}$$

We take p as an explicit function of R, i.e., $p=p_0e^{-\check{k}R}$, where $\check{k}$ and p_0 are constants. Using the value of p in Eq.(12), we find

$$\rho=\frac{\zeta}{R^2}+\frac{2(1+\check{k}R)p_0e^{-\check{k}R}}{\check{k}^2R^2}, \tag{40}$$

where ζ is the constant of integration. Inserting the values of p and ρ in Eq.(39), we obtain

$$V(\varphi) = \frac{\zeta}{2R^2}-\frac{p_0e^{-\check{k}R}}{2}\left(1-\frac{2(1+\check{k}R)}{\check{k}^2R^2}\right), \tag{41}$$

$$\dot{\varphi}^2 = \frac{\zeta}{R^2}+p_0e^{-\check{k}R}\left(1+\frac{2(1+\check{k}R)}{\check{k}^2R^2}\right), \tag{42}$$

which satisfy the KG equation. Using Eqs.(40)-(42) in (28), it follows that

$$V_{eff_{(1)}}(R) = 1-\left(\frac{2R^3}{(R^2+e^2)^{\frac{3}{2}}}\right)^2\left(\frac{M_+-M_-}{m}\right)^2-\frac{(M_++M_-)R^2}{(R^2+e^2)^{\frac{3}{2}}} - \left(\frac{m}{2R}\right)^2, \tag{43}$$

$$V_{eff_{(2)}}(R) = 1-\left(\frac{2R^3}{R^3+2e^2}\right)^2\left(\frac{M_+-M_-}{m}\right)^2-\frac{(M_++M_-)R^2}{(R^3+2e^2)} - \left(\frac{m}{2R}\right)^2, \tag{44}$$

$$V_{eff_{(3)}}(R) = 1-\left(\frac{2R^3}{(R^2+e^2)^{\frac{3}{2}}}\right)^2\left(\frac{M_+-M_-}{m}\right)^2-\frac{(M_++M_-)R^2}{(R^2+e^2)^{\frac{3}{2}}} + \frac{e^2R^2}{(R^2+e^2)^2}-\left(\frac{m}{2R}\right)^2, \tag{45}$$

where

$$m=4\pi R^2\rho\equiv 4\pi\zeta+\frac{8\pi p_0e^{-\check{k}R}}{\check{k}^2}(1+\check{k}R). \tag{46}$$

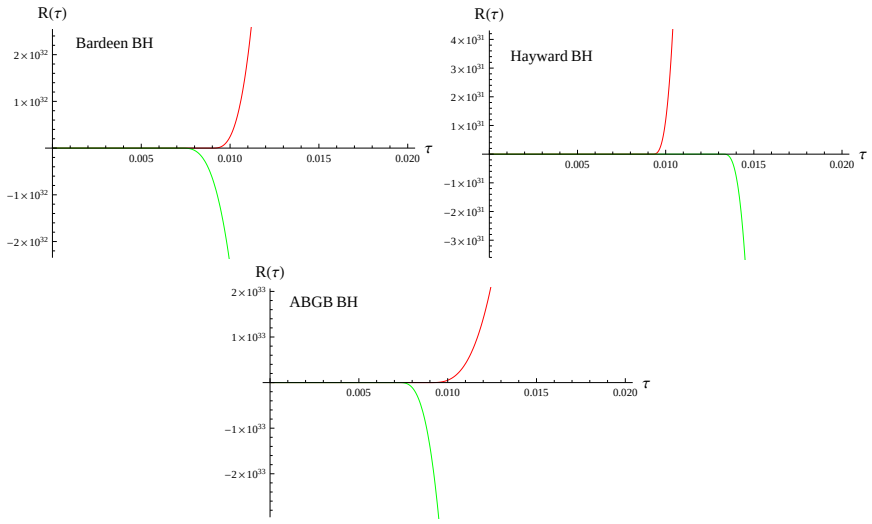

Figure 12: Plots of the shell radius in massive scalar field.

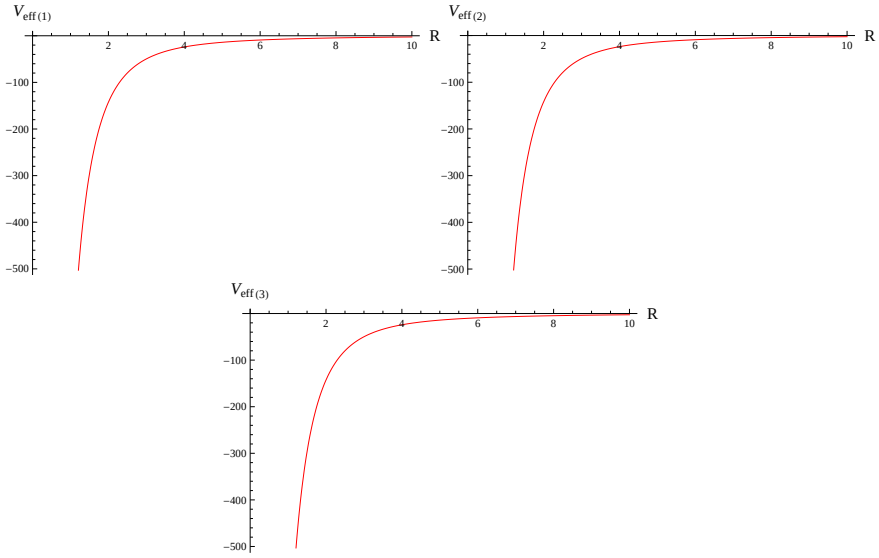

Figure 13: Behavior of V_{eff} of a massive scalar shell. The plots for Bardeen (left) and Hayward (right) is given in the upper panel while the graph of ABGB BH is in the lower panel.

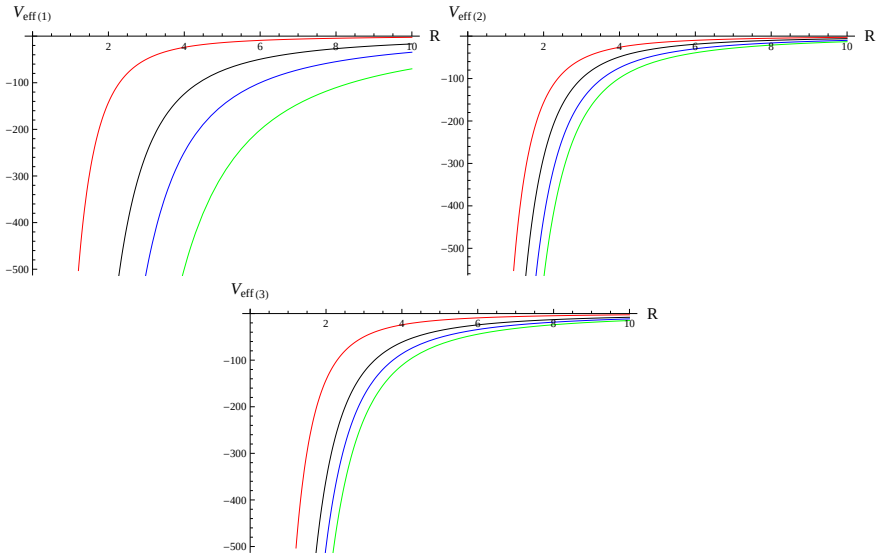

Figure 14: plots of V_{eff} of the massive scalar shell by using different values of e.

Figures **12-14** show the behavior of thin-shell for the massive scalar field for $M_- = 0$, $M_+ = 1$, $R_0 = p_0 = \check{k} = 1$, $e = 1$ and $\zeta = 3$. Figure **12** describes the nature of the shell radius for the massive scalar field. The upper curve corresponds to constant motion which leads to expansion of the shell with the increasing time. The lower curve follows the same initial configuration leading the shell to collapse. Figures **13** and **14** illustrate the behavior of effective potential for the massive scalar field with fixed mass and varying the charge parameter. In Figure **13**, we see that the effective potential diverges for the initial data. This negative effective potential indicates that the gravitational forces lead the shell to collapse. In Figure **14**, the effective potential is plotted for different values of charge parameter which shows that the shell collapses for all values of charge.

4 Final Remarks

In this paper, we have examined the dynamics of spherically symmetric scalar thin-shell (both massless and massive scalar fields) by taking regular geometry for the interior as well as exterior regions. We have considered three

regular BHs, Bardeen, Hayward and ABGB. The equation of motion (16) and the KG equation (27) can completely describe the dynamical behavior of the shell. We have discussed solutions of these equations graphically shown in Figures **1**-**5** which represent both collapse and expansion of the shell. The charged and uncharged shell provide a comparison between the shell's motion of singular and non-singular BHs, respectively. Initially the velocity of the shell with respect to stationary observer in regular spacetime is slower as compared to the Schwarzschild case (Figures: **1**-**3**). It is found that the scalar field increases for the case of collapse while for expansion it shows decreasing behavior for all BHs (Figures: **4**-**5**).

In massless case, the increase or decrease in shell's radius along the proper time represents that the shell expands continuously or collapses (Figure **6**). The motion of the shell is determined by the effective potential (Figures **7**-**11**). The shell is partitioned into two regions by a saddle point ($V_{eff} = 0$) which expands forever in the region $V_{eff} > 0$ while the region with $V_{eff} < 0$ indicates the collapsing shell. For massive scalar field, the behavior of the shell radius shows that it either expands forever or undergoes collapse (Figure **12**). The effective potential (Figure **13** and **14**) is always negative for the fixed mass (interior and exterior) with different values of e. These results indicate that the massive scalar shell always collapse to zero size for the considered parameters. We conclude that there are three possibilities in the dynamical evolution of the scalar thin-shell: continuous expansion ($V_{eff} > 0$), stable configuration ($V_{eff} = 0$) and gravitational collapse ($V_{eff} < 0$).

References

Ayon-Beato. E., Garcia A.: Phys. Rev. Lett. **80**, 5056 (1998)
Bardeen, J.: Proceedings of GR5 (Tiflis, USSR, 1968), p 174
Barrabès, C., Israel, W.: Phys. Rev. D **43**, 1129 (1991)
Bergmann, Q., Leipnik, R.: Phys. Rev. **107**, 1157 (1957)
Bhattacharya, S., Goswami, R., Joshi, P.S.: arXiv:0807.1985
Borde, A.: Phys. Rev. D **50**, 3692 (1994)
Borde, A.: Phys. Rev. D **55**, 7615 (1997)
Boulware, D.G.: Phys. Rev. D **8**, 2363 (1973)
Brill, D.R., Wheeler, J.A.: Phys. Rev. **29**, 465 (1957)
Bronnikov, K.A.: Phys. Rev. Lett. **85**, 4641 (2000)
Bronnikov, K.A.: Phys. Rev. D **63**, 044005 (2001)

Chase, J.E.: Nuovo Cimento B **67**, 136 (1970)
Choptuik, M.W.: Phys. Rev. Lett. **70**, 9 (1993)
Christodoulou, D.: Commun. Pure Appl. Math. **44**, 339 (1991)
Crisostomo, J., Olea, R.: Phys. Rev. D **69**, 104023 (2004)
Frederick, J., Ernst, Jr.: Phys. Rev. **105**, 1662 (1957)
Gleiser, M.: Phys. Rev. D **38**, 2376 (1988)
Goncalves, S.M.C.V.: Phys. Rev. D **66**, 084021 (2002)
Harada, T., Chiba, T., Nakao, K., Nakamura, K.: Phys. Rev. D **55**, 2029 (1997)
Hayward, S.A.: Phys. Rev. Lett. **96**, 031103 (2006)
Israel, W.: Nuovo Cimento B **44**, 1 (1966)
Israel, W.: Nuovo Cimento B **48**, 463 (1967)
Kaup, D.J.: Phys. Rev. **172**, 1331 (1968)
N*úñ*ez, D., Quevedo, H., Salgado, M.: Phys. Rev. D **58**, 083506 (1998)
N*úñ*ez, D.: Astrophys J. **482**, 963 (1997)
Oren, Y., Piran, T.: Phys. Rev. D **68**, 044013 (2003)
Ruffini, R., Bonazzola, S.: Phys. Rev. **187**, 1767 (1969)
Seidel, E., Suen, W.: Phys. Rev. D **42**, 384 (1990)
Sharif, M., Abbas, G.: Gen. Relativ. Gravit. **43**, 1179 (2011)
Sharif, M., Abbas, G.: Gen. Relativ. Gravit. **44**, 2353 (2012)
Sharif, M., Ahmad, Z.: Int. J. Mod. Phys. A **23**, 181 (2008)
Sharif, M., Iqbal, K.: Mod. Phys. Lett. A **24**, 1533 (2009)
Siebel, F., Font, J.A., Papadopoulos, P.: Phys. **65**, 024021 (2001)
Wheeler, J.A.: Phys. Rev. **97**, 511 (1955)